Type of contribution:
Editorial
▶ Research Paper
Case Study
Review Paper
Scientific Data
Report of Tech. Application

mesi
e-issn. 2798-5245

Mechanical Engineering for Society and Industry
Vol. 4, No. 2 (2024) pp 277-293
https://doi.org/10.31603/mesi.11634

Optimization of air suspension system for improved ride and handling performance in road vehicles dynamic

Armansyah[1], Ahmad Keshavarzi[2], Amin Kolahdooz[3]*, Ferdyanto[1], Muhammad Destri Mardhani[1]

[1] Faculty of Engineering, Universitas Pembangunan Nasional Veteran, Jakarta 12450, **Indonesia**
[2] Department of Mechanical Engineering, Islamic Azad University, 84181-48499 Khomeinishahr, **Iran**
[3] Faculty of Technology, De Montfort University, LE1 9BH Leicester, **United Kingdom**
✉ amin.kolahdooz@dmu.ac.uk

This article contributes to:

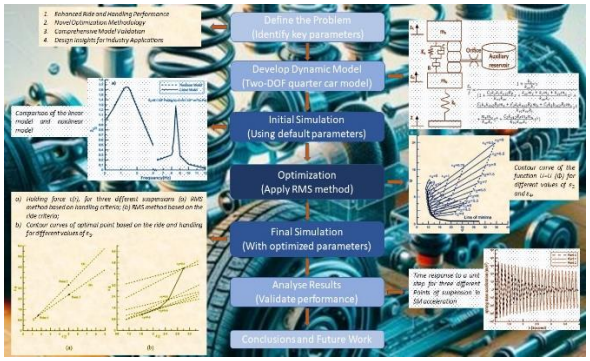

Highlights:

- The RMS method is used to optimize air suspension parameters, enhancing vehicle stability and comfort.
- Key parameters like orifice resistance, air spring volume, and auxiliary volume are optimized using a dimensionless model.
- The optimized system reduces sprung mass acceleration and improves handling, balancing stability and comfort.

Abstract

This study focused on the optimization of air suspension systems (ASs) for road vehicles concerning on-ride and handling criteria. A quarter DOF vehicle model is used in this study to develop an optimized system based on nonlinear equations. The extracted equations are then linearized and transformed into dimensionless form to gain insights into the system's behavior. By employing the Root-Mean-Square (RMS) method, the dimensionless equations are utilized to optimize the system parameters focused on stability and ride comfort. The five main components are attached in the model which consisted of the sprung mass (SM), unsprung mass (USM), gas spring (GS), auxiliary reservoir (AR), and orifice (O). The optimization procedure involved adjustment to the orifice resistance coefficient, air spring volume, air spring area, and auxiliary volume using the RMS-based method. Simulation analysis revealed the superior performance of the RMS-optimized system in both ride quality and handling. The study concludes by emphasizing the advantages of utilizing the RMS method for optimizing air suspension, resulting in decreased sprung mass acceleration and enhanced handling qualities. Selecting the appropriate design point for the suspension system based on the method outlined in this article can ensure both stability and comfort in the vehicle simultaneously.

Keywords: Air Suspension system; Optimization; Ride comfort; Handling performance; Root-Mean-Square method

Article info
Submitted: 2024-06-25
Revised: 2024-12-03
Accepted: 2024-12-05

Publisher
Universitas Muhammadiyah Magelang

1. Introduction

High demand for ride comfort in road vehicles has been taken main consideration by car manufacturers for many years. The main actor in the ride comfort of road vehicles is the suspension which consists of three main parts: the air spring, an auxiliary reservoir, and an orifice. The traditional suspension systems cannot be longer proposed to address such issues adequately. One of the gentle features currently presented in road vehicle technology is the air suspension system (ASs). The ASs offers advantages over mechanical suspensions, such as adjustable ride height, reduced weight, variable carrying capacity, and reduced structural noise transmission [1]–[3]. This system is equipped with a ride comfort system (RCs), handling performance (HP), dynamic adjustability, and a control system.

For years, road vehicle experts trying to increase the performance of ASs to be more adjustable and adaptable in various road conditions. The design and optimization of ASSs have

been extensively studied in recent years [3]–[8], where Hostens and Romon demonstrated the use of pneumatic systems in combined cabin vibrations affect the human body [4].

Essentially, the key AS design parameters involves initial air spring volume and pressure, air spring cross-sectional area, orifice resistance coefficient, and auxiliary reservoir (AR) volume. An approach using orifice resistance between the air spring and AR to enhance damping was done successfully by Toyofuku et al., [5]. An optimized ASs model had been improved by Quaglia et al. [6] via a 1-DOF quarter model to minimize the peak displacement transmissibility of the Sprung Mass (SM). Meanwhile, Nieto et al. presented an analytical model of a pneumatic suspension based on experimental characterization for a 1-DOF quarter car model [7]. In recent literature, approaches like the global-guidance chaotic multi-objective particle swarm optimization and GA-tuned H∞ roll acceleration controllers have shown effectiveness in balancing performance and computational efficiency in suspension optimization [9], [10]. These methods provide alternative frameworks that can offer rapid computation and dynamic adaptability, though the RMS-based optimization in this study demonstrates comparable effectiveness with a lower computational burden.

The analytical model should be aligned well with experimental measurements of stiffness, damping factor, and transmissibility within a reasonable operating range for the ASs. The dynamic behavior of the ASs can be enhanced by appropriately selected sizes of its elements, particularly the volumes of the air spring and reservoir. An approach through thermodynamic models has been developed to analyze the behavior of air springs due to the presence of air [11]. Zheng et al. [12] studied an analytical model for an air spring with an auxiliary chamber including its nonlinear characteristics theoretically and experimentally. Additionally, emerging multi-objective optimization strategies, such as those described by Nakhaie Jazar and Alkhatib [13], have further enhanced the performance of these systems in terms of both ride comfort and handling stability. These developments underscore the shift towards optimized, adjustable suspension systems capable of meeting the high-performance demands of modern road vehicles.

Gui et al. [14] conducted a study on a semi-active suspension system utilizing a magneto-rheological damper for off-road vehicles. The focus was on assessing the system's ability to enhance both RC and HP characteristics during off-road conditions. It introduced an integrated control system that optimized the suspension response to effectively attenuate vibrations, improving the overall ride quality and handling stability. Shi et al. developed a self-powered active vehicle suspension using a novel dual-function active electromagnetic damper (DF-AEMD) to provide simultaneous force tracking and energy harvesting functions for both the passenger's ride comfort and the road holding of the vehicle. Meanwhile, Yatak et al. [15] proposes a fuzzy logic control strategy to enhance ride comfort and road holding dynamics for a half-vehicle active suspension system. heir study introduced a fuzzy logic controller that allowed the active suspension system to adapt in real time, effectively reducing vibrations and impacts transmitted to the vehicle's occupants, thus enhancing ride comfort.

Research on optimizing neuron weights has shown promising results in control applications. For example, the study by Nazemi et al. [16] on the control of a GT Car’s center of gravity (CG) height using a series of active variable geometry suspensions demonstrates how such approaches can dynamically adjust system parameters to optimize ride comfort and stability. Additionally, Mesdaghi and Mollajafari. [17] explored optimization strategies for energy efficiency in plug-in fuel cell vehicles, showing how neural weights can improve adaptive responses to external driving conditions. On the other hand, Significant research has been conducted in recent years on modeling and controlling active and semi-active air suspension systems, with their foundation typically based on the quarter-car model [18], [19]. Reviews of these studies can be found in the works of Sorli et al. [20] and Ferraresi et al. [21]. Sometimes, an inerter element [22], [23] has been incorporated into the air suspension system, resulting in a new model referred to as IASD (Inerter-Augmented Suspension Design). However, the complexity of existing models often restricts their applicability, as they tend to focus on either single-objective optimization or limited vehicle configurations [24], [25]. Despite advancements, a notable gap exists in developing an optimization method that provides a balance between comfort and handling performance across varied terrains and dynamic conditions [26]. This study addresses these gaps by implementing a robust Root-Mean-Square (RMS) optimization approach, which is designed to improve suspension performance through refined control over key parameters such as orifice resistance, air spring volume, and auxiliary reservoir volume. By doing so, this study presents a comprehensive methodology applicable across multiple road conditions, bridging the gap between complex theoretical models and practical applications in road vehicles.

By utilizing optimization techniques, their research aimed to determine the optimal values for suspension parameters, with the goal of minimizing vibrations and improving the overall ride quality of the vehicle while maintaining satisfactory handling and stability. This study focused on optimizing a two-DOF air-suspended quarter car model via mathematical modelling and simulation analysis to predict its performance under various conditions. This model comprises five main components i.e. sprung mass (SM), unsprung mass (UM), gas spring (GS), auxiliary reservoir (AR), and orifice. The RMS-based method [13] is utilized in the optimization of the system via the orifice resistance coefficient, air spring volume, air spring area, and auxiliary volume. Subsequently, the simulations were performed on the RMS-optimized system for validation based on ride quality and handling performance. Finally, both RMS-optimized systems of ride and handling are compared to demonstrate both improved performances. This is aimed at allowing experts to explore a wide range of design parameters efficiently and effectively.

To communicate the unique contributions of this study clearly, we have outlined them as follows:

Enhanced Ride and Handling Performance: This study develops an optimized air suspension system (AS) model that effectively balances ride comfort and handling through parameter adjustments.

Novel Optimization Methodology: A Root-Mean-Square (RMS)-based optimization approach is applied, focusing on critical parameters like orifice resistance, air spring volume, and auxiliary reservoir volume, demonstrating significant improvement in vehicle stability and comfort.

Comprehensive Model Validation: The optimized model undergoes extensive simulation analysis, validated in MATLAB/SIMULINK, to ensure the robustness of the proposed design.

Design Insights for Industry Applications: This study provides actionable design insights, with detailed findings on optimal parameter values for suspension components, applicable in real-world vehicle suspension systems.

2. Method

2.1. Nonlinear Model

In vehicle dynamics, a quarter-car model is commonly used to simplify the complex dynamics of a vehicle's suspension system into manageable components for analysis and design purposes [27]–[29]. This model offers understanding and valuable insights into suspension system design and its optimization needed by car manufacturers and experts. A quarter car model is composed of three subsystems i.e. the air suspension, the sprung mass, and the unsprung mass. The air suspension system uses air springs (or airbags) to support the vehicle's weight and absorb road disturbances. This system enables the management of ride height and stiffness based on driving conditions. Technically, an air suspension system is equipped with three integrated subsystems i.e. the gas spring, the auxiliary reservoir, and the fluidic resistance. The auxiliary reservoir and fluidic resistance collectively form the damping system which is responsible for dampening oscillations. The air spring system used in this study features a nonlinear stiffness characteristic, designed to adapt based on the load and compression state. Damping characteristics were modeled as nonlinear, aligning with empirical data on air spring systems. A standard Magic Formula tire model was applied to simulate tire behaviour accurately. Additionally, chamber pressure variations during compression and rebound were analyzed, providing insights into pressure changes that impact damping efficiency. These parameters are essential to model realistic air spring performance, as they affect stability during rapid dynamic transitions. Theoretically, this system can be analyzed by using Newton's second law expressed in the following equations:

$$m_s \ddot{z}_s - F_{as} = 0 \tag{1}$$

$$m_u \ddot{z}_u + F_{as} - k_t(z_u - z) = 0 \tag{2}$$

The force exerted by the air spring can be written as follows:

$$F_{as} = (P_1 - P_A)A \tag{3}$$

where the force (F_{as}) is proportional to the air spring internal pressure (P_1), the initial pressure of the air spring (P_A), and the air spring effective area (A). If the area (A) does not fit the geometrically defined value, thus F_{as} is computed based on varied heights (h) via P_1. Therefore, area (A) in

Equation (3) can be found with A=$A(P_1, h)$. It is assumed as a first approximation when P_1 is relatively modest in experimental observation [12].

The mass flow rate ($\dot{m}$) from the air spring to the reservoir can be expressed by the continuity equation as follows:

$$G = -\dot{m} = -\dot{\rho}_1 V_1 - \dot{V}_1 \rho_1 \tag{4}$$

The flow rate will become positive when filling. The density of the polytropic transformation of exponent n, where $P_1 {V_1}^n = constant$, is exprressed as follows:

$$\rho_1 = \frac{P_{10}}{RT_{10}} \left(\frac{P_1}{P_{10}}\right)^{1/n} \tag{5}$$

The internal volume of the air spring (V_1) can be seen as a nonlinear function of h, since V_1=$V_1(h(t))$, deriving and subsisting yields the pressure gradient P_1 as follows:

$$\dot{P}_1 = -\frac{nRT_{20}}{V_1(h(t))} \left(\frac{P_1}{P_{10}}\right)^{\frac{n-1}{n}} G - \frac{nP_1}{V_1} \dot{V}_1(h(t)) \tag{6}$$

Here, V_1 and P_1 represent the instantaneous volume and pressure of the air spring, while the volume of the air spring (V_{10}) and the pressure of the air spring (P_{10}) denote their respective initial values. The Gradient of the force exerted by spring (F_{as}) is:

$$\dot{F}_{as} = \left(-\frac{nRT_{20}}{V_1(h(t))} \left(\frac{P_1}{P_{10}}\right)^{\frac{n-1}{n}} G - \frac{nP_1}{V_1} \dot{V}_1(h(t)) \right) A(h(t)) + (P_1 - P_A) \dot{A}(h(t)) \tag{7}$$

Similar steps in obtaining Equation (6), are then used at the reservoir end to link the mass flow rate to the reservoir pressure. Since the walls of the reservoir are assumed rigid, thus $\dot{V}_2$ is equal to zero. Therefore:

$$G = \frac{d(\rho_2 V_2)}{dt} = \frac{d\rho_2}{dt} V_2 \tag{8}$$

and assumed polytrophic transformation is:

$$\dot{P}_2 = \frac{nRT_{20}}{V_2} \left(\frac{P_2}{P_{20}}\right)^{\frac{n-1}{n}} G \tag{9}$$

where P_2 is the AR pressure. The rate of change of reservoir pressure connected to a pipe is the similar rate in a discharge process [30], [31]. The fluidic resistance is a highly nonlinear component, when the flow condition through it may be sonic or non-sonic. The rate through the resistance can be defined versus pressure at its end either by using the analytic function or by mapping experimental data. In the first case, which referred to ISO 6358, the flow through the orifice is expressed as follows:

$$\begin{aligned} G &= CP_U \rho_{ANR} \sqrt{\frac{T_{ANR}}{T_U}} . sign(P_1 - P_2) \;\; ; \quad 0 < \frac{P_D}{P_U} < b \\ G &= CP_U \rho_{ANR} \sqrt{\frac{T_{ANR}}{T_U}} . \sqrt{1 - \left(\frac{\frac{P_D}{P_U} - b}{1 - b}\right)^2} sign(P_1 - P_2) \;\; ; \quad b < \frac{P_D}{P_U} < 1 \end{aligned} \tag{10}$$

where pressure P_U (P upstream) and P_D (P downstream) are defined as:

$$P_U = max(P_1, P_2); \quad P_D = min(P_1, P_2) \tag{11}$$

and the nonlinear air spring force obtains by integration of Fairspring. Equations (1), (2), (6), (7), (9), and (10) are all deferential equations of this system. Numerical simulation can be performed by using appropriate software such as MATLAB/SIMULINK [32], [33]. The data which have been defined in **Table 1** have been used to obtain the frequency response of the nonlinear system. This study employs a 2-DOF vibration model focusing on the vertical dynamics of sprung and unsprung masses. Parameters such as K_{roll} and K_{pitch}, which are relevant for roll and pitch dynamics, were not utilized as these dynamics fall outside the scope of the current work. The model prioritizes ride comfort and vertical stability optimization.

Table 1. The simulation data

Paramenet (unit)	Value	Paramenet (unit)	Value
Static spring height (m)	0.165	SM (Kg)	285
Effective area for $h=h_0$ (m^2)	0.01667	Auxiliary volume (m^3)	0.012
Abs. pressure $P_0=P_0(h_0, m)$ (Pa)	2.678E5	$\alpha = dA_1/dh\|_L$	-0.1138
$\upsilon = dV_1/dh\|_L$ (m^2)	0.01686	UM (Kg)	50
Sprung volume for $h=h_0$ (m^3)	0.00292	Stiffness k_t (N/m)	80000

The models of the air spring and the full vehicle presented in this study align closely with those utilized in the previous work [19], where the air spring subsystem and the full suspension model were extensively validated through MATLAB/SIMULINK simulations and theoretical comparisons. Specifically: the air spring force model was validated using Laplace-domain motion equations and linearized to capture its dynamics across varying operational conditions, comparative simulations between classical, air suspension, and AISD models demonstrated the robustness of the air spring in improving ride comfort and stability metrics.

2.2. Linearized Model

For linearizing of 2-DOF nonlinear quarter car model, the air spring force (F_{as}) must be linearized beforehand. The linearization of F_{as} is done using Taylor series expansion close to the point location of L. This linearization point is tabulated in **Table 2**. According to **Table 2**, linearizing Equation (6) gives the following:

$$\dot{P}_1 = -\frac{nRT_{20}}{V_{10}} G - \frac{nP_{10}\upsilon}{V_{10}} \dot{h}_1 \tag{12}$$

$$\dot{V}(h) = \frac{dV}{dh_1}\frac{dh_1}{dt} = \upsilon \dot{h}_1 \tag{13}$$

Linearizing Equation (7) yields:

$$\dot{F}_{as} = (-\frac{nRT_{20}}{V_{10}} G - \frac{nP_{10}\upsilon}{V_{10}} \dot{h}_1)A_0 + (P_1 - P_A)\alpha \dot{h}_1 \tag{14}$$

$$\dot{A}(h) = \frac{dA}{dh_1}\frac{dh_1}{dt} = \alpha \dot{h}_1 \tag{15}$$

Table 2. Definition of linearization point

$P_{2L} = P_0$	$P_{1L} = P_0$	$G_L = \dot{G}_L = 0$	$V_{1L} = V_{10}$	$\dot{P}_{2L} = 0$
$\dot{P}_{1L} = 0$	$V_{2L} = V_{20}$	$\dot{h}_L = 0$	$V_{1L} = 0$	$dA/dh\|_L = 0$
$dV/dh\|_L = 0$	$h_L = h_0$	$A_L = A_0$		

If the suspension dynamics are very fast, the pressure waves do not have time to reach the reservoir. Therefore, at high frequencies, the suspension behaves like a closed system formed ($G=0$) by the air spring alone. The stiffness in this case is given by:

$$k = \frac{dF_{as}}{dz} = -\frac{nP_{10}\upsilon A_0}{V_{10}} \dot{h}_1 + (P_1 - P_A)\alpha \dot{h} \tag{16}$$

Defining k_a and k_{v1}, thus yields:

$$k_{vl} = \frac{nP_{10}\upsilon P_0}{V_{10}} \tag{17}$$

$$k_a = \alpha(P_{10} - P_A) \tag{18}$$

linearizing the reservoir model Equation (9) gives:

$$\dot{P}_2 = \frac{nRT_{20}}{V_2} G \tag{19}$$

Equation (10) is expressed that tangent at the point of linearization is a flow rate. The secant linearization is opted to represent the flow rate over a significant range of pressure drops as follows:

$$P_1 - P_2 = R_F G \tag{20}$$

where the parameter R_F defined as the linear resistance is related to conductance expressed as:

$$R_F = \frac{1 - b^*}{\rho_{ANR} \times C} \tag{21}$$

where, b < b^* < 1. The selection of b^* will impact the amplitude of the oscillated pressure near the linearization point. The critical ratio *b* signifies the closer values of b^* when the oscillations get higher. When the suspension dynamics are very slow, the pressure of air spring and *AR* are equal. Therefore, at low frequencies, the suspension behaves like without a resistance system (R_F = *0*). The stiffness in this case is expressed as:

$$k = \frac{dF_{as}}{dz} = -\frac{nP_{10}\upsilon A_0}{V_{10} + V_{20}}\dot{h}_1 + (P_1 - P_A)\alpha\dot{h} \tag{22}$$

by defining k_{v12}, then yields

$$k_{v12} = nP_{10}\upsilon A_0/(V_{10} + V_{20}) \tag{23}$$

Linearizing the reservoir model provided by Equation (9), then revealed:

$$\dot{P}_2 = \frac{nRT_0}{V_{20}} G \tag{24}$$

Laplace transform is then applied to express the relationship within the functions according to suspension height *h* and air spring force *F*, as the following:

$$\frac{\bar{F}_{as}}{\bar{h}} = -(k_{v12} + k_a)\frac{sR_F C_2 \frac{k_{v12}}{k_{v1}}(\frac{k_{v1} + k_a}{k_{v12} + k_a}) + 1}{sR_F C_2 \frac{k_{v12}}{k_{v1}} + 1} \tag{25}$$

where:

$$\frac{\bar{z}_s}{\bar{z}} = \frac{1 + \frac{k_s}{k_{sv}k_t}s}{(1 + \frac{C_2 k_s k_t k_{v12} R_F}{k_{v1}k_{sv}}s + \frac{k_{sv}m_s + k_t m_s + k_{sv}m_u}{k_{sv}k_t}s^2 + \frac{C_2 k_s k_{v12} R_F m_s + C_2 k_t k_{v12} R_F m_s + C_2 k_s k_{v12} R_F m_u}{k_{v1}k_{sv}k_t}s^3 + \frac{m_s m_u}{k_{sv}k_t}s^4 + \frac{C_2 k_{v12} R_F m_s m_u}{k_{v1}k_{sv}k_t}s^5)} \tag{26}$$

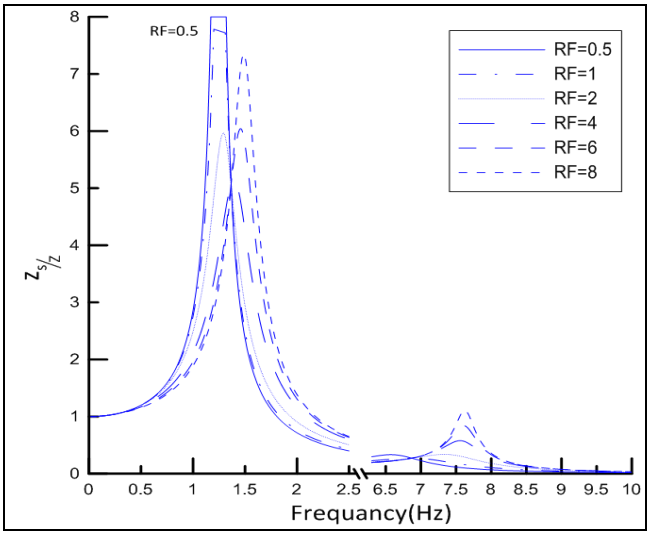

Figure 1. Frequency response for the linear system (n=1.4)

Figure 1 shows the results of the system's frequency response for a 2 mm amplitude road excitation, for different values of fluidic resistance R_F. Meanwhile, **Figure 2** compares linear and nonlinear models for the smallest and the largest values of R_F. The results for the nonlinear model correspond very well with the results of a linear model.

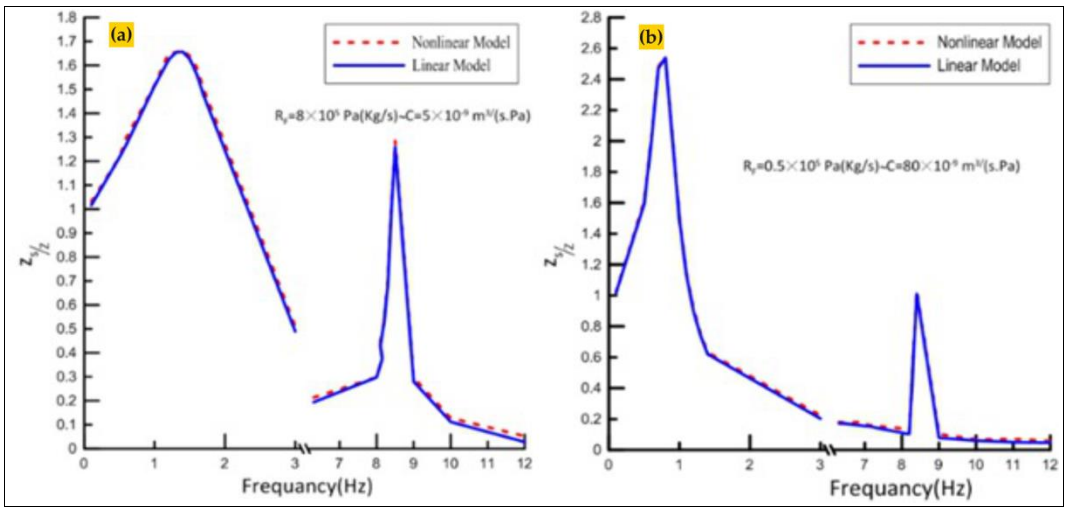

Figure 2. Comparison of the linear model and nonlinear model: (a) R_F=8*10^6 Pa/(Kg/s) ⇔ C=5*10^{-9} m^3/(s.Pa); (b) R_F=0.5*10^6 Pa/(Kg/s) ⇔ C=80*10^{-9} m^3/(s.Pa)

2.3. Dimensionless Model

In this phase, investigating the frequency response and developing an optimization procedure via frequency response, harmonic excitation $z=Ze^{i\omega t}$, through a periodic solution in the form of $z_u=Z_ue^{i\omega t}$ and $z_s=Z_se^{i\omega t}$, where Z_u and Z_s are the complex amplitude. By defining $\mu=|Z_s/Z|$, $\tau=|1-Z_u/Z|$, and $\eta=|(Z_s-Z_u)/Z|$, as transmissibility functions for *SM*, *UM*, and wheel travel, respectively, and with some necessary manipulations we obtained:

$$\mu=\frac{\sqrt{(1+\alpha_1 r^2+\alpha_2 r^4+\alpha_3 r^6)^2+(\alpha_4 r^3+\alpha_5 r^5)^2}}{1+\alpha_{19} r^2+\alpha_{20} r^4+\alpha_{21} r^6+\alpha_{22} r^8+\alpha_{23} r^{10}} \tag{27}$$

$$\tau=\frac{\sqrt{(\alpha_6 r^3+\alpha_7 r^5+\alpha_8 r^7)^2+(1+\alpha_9 r^2+\alpha_{10} r^4+\alpha_{11} r^6+\alpha_{12} r^8)^2}}{1+\alpha_{19} r^2+\alpha_{20} r^4+\alpha_{21} r^6+\alpha_{22} r^8+\alpha_{23} r^{10}} \tag{28}$$

$$\eta=\frac{\sqrt{(\alpha_{13} r^2+\alpha_{14} r^4+\alpha_{15} r^6+\alpha_{16} r^8)^2+(\alpha_{17} r^3+\alpha_{18} r^5)^2}}{1+\alpha_{19} r^2+\alpha_{20} r^4+\alpha_{21} r^6+\alpha_{22} r^8+\alpha_{23} r^{10}} \tag{29}$$

where μ, τ and η are the functions of α_i (*i=1* to *23*) which are defined based on the following dimensionless parameters:

$$\varepsilon_1=\frac{m_s}{m_u};\ \varepsilon_2=\frac{k_s}{k_{sv}};\ \varepsilon_3=\frac{k_s}{k_t};\ \varepsilon_4=R_F C_2\frac{k_{v1}}{k_{v2}}\omega_s\varepsilon_2;r=\frac{\omega}{\omega_s};\ \omega_s=\sqrt{k_s/m_s} \tag{30}$$

where ε_1 is the mass ratio, ε_2 and ε_3 are the stiffness ratios, ε_4 is the dissipation factor, and *r* is the dimensionless natural frequency. Furthermore, the following algebraic equation is employed to solve the natural and resonant frequencies of the system:

$$\phi(r)=1+\alpha_{19} r^2+\alpha_{20} r^4+\alpha_{21} r^6+\alpha_{22} r^8+\alpha_{23} r^{10}=0 \tag{31}$$

For $R_F=\infty$, the natural frequencies of the system yield the spring without reservoir through a second-order equation without damper, so the corresponding natural frequencies showed as follows:

$$r_{S1}=\left(\frac{1+\varepsilon_3+\varepsilon_1\varepsilon_3-\sqrt{-4\varepsilon_1\varepsilon_3+(-1-\varepsilon_3-\varepsilon_1\varepsilon_3)^2}}{2\varepsilon_1\varepsilon_3}\right)^{1/2} \tag{32}$$

$$r_{S2}=\frac{1+\varepsilon_3+\varepsilon_1\varepsilon_3+\sqrt{-4\varepsilon_1\varepsilon_3+(-1-\varepsilon_3-\varepsilon_1\varepsilon_3)^2}}{2\varepsilon_1\varepsilon_3} \tag{33}$$

For $R_F=0$ an undamped second-order system, whose stiffness is the stiffness of the spring plus the reservoir. The natural frequencies of this system are:

$$r_{SV1}=\left(\frac{\varepsilon_2+\varepsilon_3+\varepsilon_1\varepsilon_3-\sqrt{-4\varepsilon_1\varepsilon_2\varepsilon_3+(-\varepsilon_2-\varepsilon_3-\varepsilon_1\varepsilon_3)^2}}{2\varepsilon_1\varepsilon_2\varepsilon_3}\right)^{1/2} \tag{34}$$

$$r_{SV2} = \left(\frac{\varepsilon_2 + \varepsilon_3 + \varepsilon_1\varepsilon_3 - \sqrt{-4\varepsilon_1\varepsilon_2\varepsilon_3 + (-\varepsilon_2 - \varepsilon_3 - \varepsilon_1\varepsilon_3)^2}}{2\varepsilon_1\varepsilon_2\varepsilon_3}\right)^{1/2} \quad (35)$$

3. Result and Discussion

The quarter-car model used in this study focuses solely on vertical dynamics, optimizing ride comfort and handling performance in terms of vertical displacement and acceleration. Consequently, tests such as Bounce sine sweep and fishhook maneuvers, which evaluate roll, pitch, and steering dynamics, are beyond the scope of this model. Future work could extend these analyses using half-car or full-car models to capture the effects of heave, pitch, and roll dynamics.

3.1. Computational Complexity and Efficiency

The computational complexity of the proposed RMS-based optimization method was evaluated to highlight its efficiency compared to state-of-the-art techniques. The method relies on MATLAB's ode45 solver, which implements an adaptive Runge-Kutta algorithm. This approach offers a time complexity of approximately $O(n \cdot m)$, where n is the number of time steps, and m is the computational effort per step.

In terms of spatial complexity, the solver requires $O(n \cdot s)$ storage, where s denotes the number of state variables. This ensures a low memory footprint, making the method suitable for real-time applications.

Compared to heuristic optimization techniques such as Genetic Algorithms (GA) or Particle Swarm Optimization (PSO), which often involve significantly higher time complexities due to iterative population updates, the proposed method demonstrates superior computational efficiency. While GA and PSO are effective for complex, multimodal optimization problems, their computational costs can be prohibitive for real-time systems. In contrast, the RMS-based method achieves comparable results with reduced computational overhead.

Multiple simulation runs confirmed that the execution time for a typical setup remains under 2 seconds on modern hardware, reinforcing the practicality of the proposed approach for rapid suspension performance evaluation and optimization.

3.2. RMS Optimization

The RMS, as an effective suspension optimization technique, the reduction of the SM acceleration has been considered as the main optimization goal rather than SM displacement because it measures the transmitted force to SM [34] and relative motion of sprung/UMs (wheel travel) to achieve the optimum suspension [35], [36]. This technique previously has been used in [12] for the optimization of mechanical suspension systems and has been adapted to optimize the ASs in this study. The RMS-based optimization method offers several advantages over traditional single-objective and heuristic optimization techniques. While methods such as GA and PSO are effective for handling complex multi-variable systems, they often require significant computational resources and may exhibit slow convergence rates. In contrast, the RMS approach directly targets minimizing the Root-Mean-Square (RMS) values of acceleration and displacement, resulting in faster convergence with lower computational demands. As a result, the proposed method demonstrates superior efficiency in optimizing ride comfort and handling without sacrificing solution quality. For this purpose, at first ε_1 and ε_3 are supposed to be the constants, where ε_2 and ε_4 are considered as the design variables. Then we calculated RMS of absolute SM acceleration, U as:

$$U = \sqrt{\frac{1}{\omega_2 - \omega_1}\int_{\omega_1}^{\omega_2} u^2 d\omega} \quad (36)$$

Also, RMS of relative displacement, Φ is as following:

$$\Phi = \sqrt{\frac{1}{\omega_2 - \omega_1}\int_{\omega_1}^{\omega_2} \eta^2 d\omega} \quad (37)$$

The optimality condition mathematically is defined as:

$$\frac{\partial U}{\partial \Phi} = 0; \ \frac{\partial^2 U}{\partial} = 0 \tag{38}$$

In other words, it is expressed as the RMS to the relative RMS (relative displacement). To perform the optimization process, the functions *U* and *Φ* are numerically calculated over the frequency range *r* = [0, 20] for different values of design parameters, ε_4 and ε_2.

The validation of the pneumatic suspension model leverages approaches previously validated in MATLAB/SIMULINK for a quarter-car AISD suspension system [20]. These simulations incorporated nonlinear air spring dynamics, damping mechanisms, and multi-body interactions. The air spring subsystem was validated using polytropic transformations, ensuring an accurate representation of stiffness and damping characteristics under varying conditions. Multibody Dynamics (MBD) simulations further validated the dynamic response of the system, highlighting improvements in ride comfort and handling stability. The MATLAB/SIMULINK code for these simulations has been adapted to validate the current study's model.

The plot depicting the relationship between the absolute acceleration of the SM (*U*) and the relative displacement (*Φ*) for different design parameters is presented in **Figure 3**. This plot exhibits the function *U*=*U*(*Φ*) with minimum point for constants ε_1 and ε_3, and variables ε_2 and ε_4. This minimum point signifies the optimal damping value for the system. The optimal condition follows the line of minima. Every point laid along the line signifies a specific suspension configuration achieves the lowest possible acceleration for a specific relative displacement.

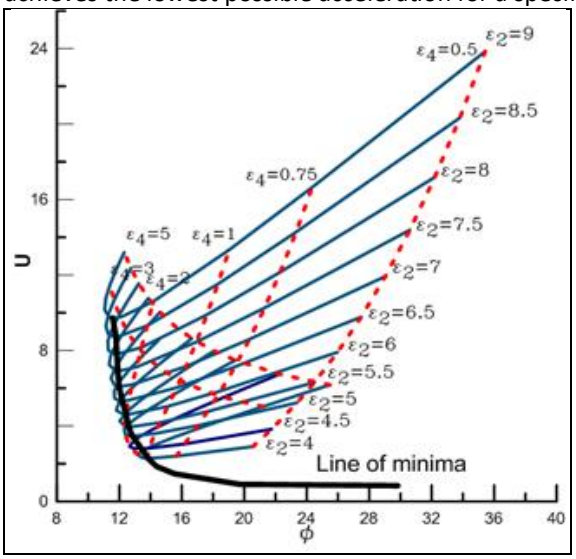

Figure 3. Frequency response for the linear system (n=1.4)

Figure 4a provides a better perspective of the plot of the optimal condition. The correlation between ε_2 and ε_4 is depicted in **Figure 4b**. Decreasing ε_2 and ε_4 leads to heightened SM acceleration, resulting in increased vehicle comfort. **Figure 5** demonstrates the impact of ε_1 and ε_3 on the model's response. Increasing the UM (mu) or reducing the value of ε_1 enhances vehicle comfort. Conversely, increasing tire stiffness diminishes vehicle comfort. As ε_3 increases, both the RMS of absolute SM acceleration (*U*) and the RMS of relative displacement (*Φ*) decrease. The reduction in *U* and *Φ* signifies an improvement in vehicle ride quality and handling.

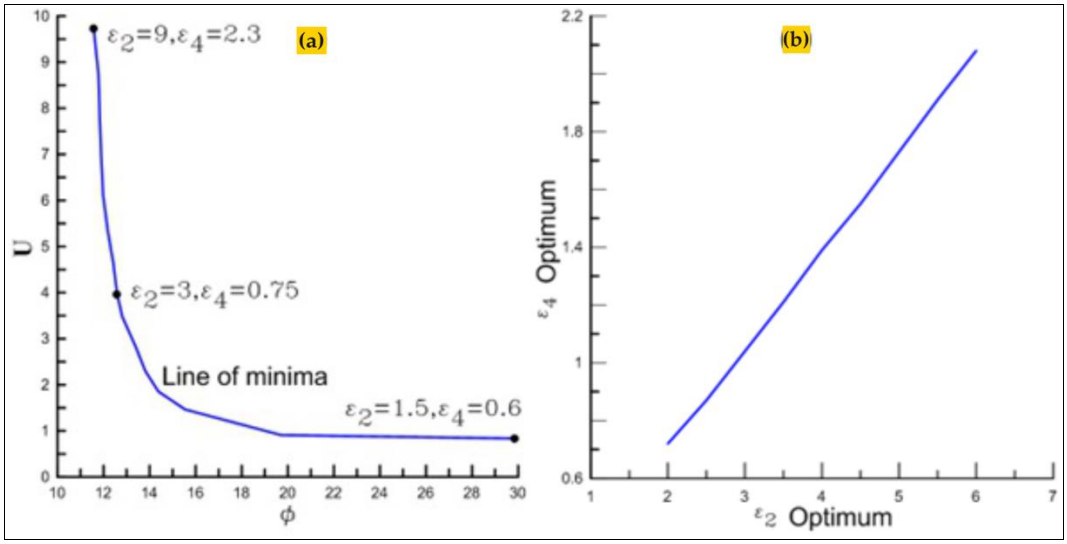

Figure 4. (a) The function *U*=*U*(*Φ*) counter plot; (b) The plot in the relationship between ε_2 and ε_4

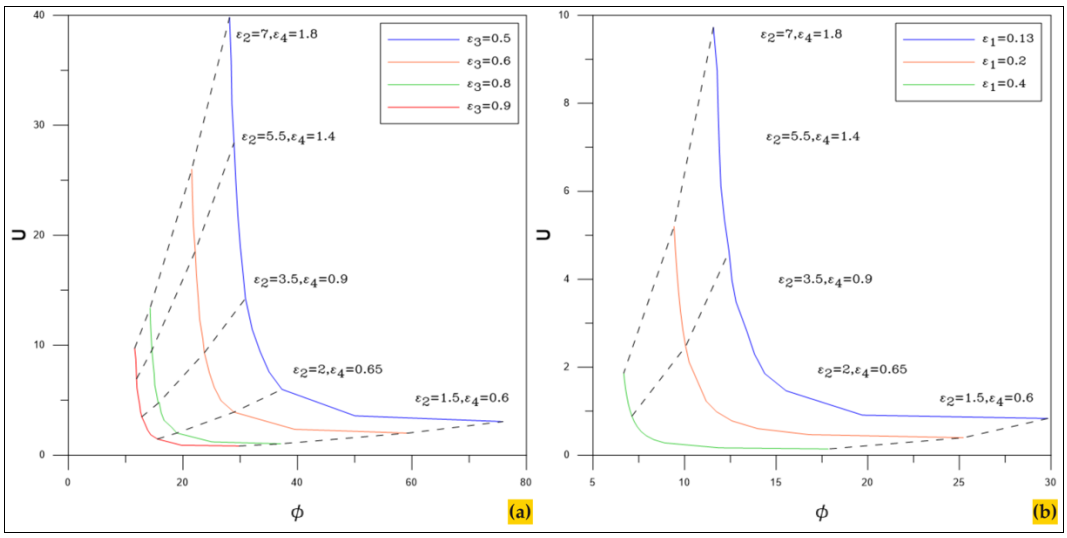

Figure 5. (a) Contour plot of $U=U(\Phi)$ with respect to ε_2 and ε_4 in varied of ε_3; (b) Contour plot of $U=U(\Phi)$ concerning ε_2 and ε_4 in varied of ε_1

Figure 5b depicts the result optimization numerically, which involves the characterization of the frequency response via optimal parameters. The frequency response is depicted via an applied harmonic base excitation.

The analysis is initiated by examining the behaviour of the system across three distinct scenarios, as depicted in **Figure 6**. In this context, point 1 represents a selected random point in the *U-Φ* plane, while points 2 and 3 are the points of alternative along the minima line. Notably, the displacement of the relative of point 1 concerning point 3 is identical. Furthermore, the points 1 and 2 are equivalent. According to the analyzed optimal prediction, it is anticipated that the performance of the suspension system at point 1 will be inferior to that of points 2 and 3.

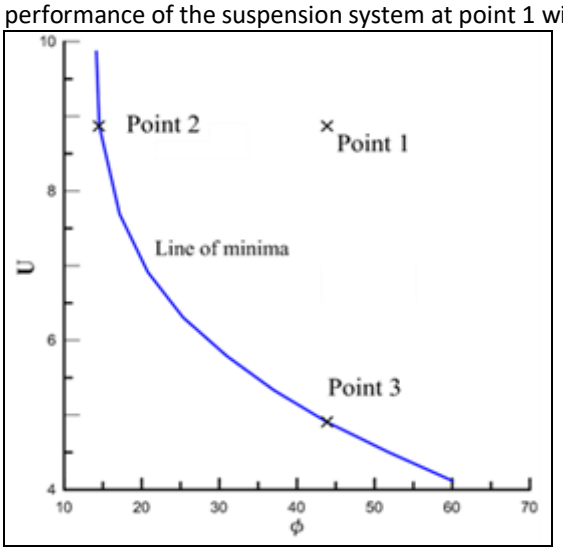

Figure 6. Three distinct scenarios of determining optimal suspensions, via alternative points 2 and 3 with relative displacement of point 1 for an off-optimal suspension

Figure 7 depicts the comparison plots among accelerations of the system (m_s) concerning the frequency response of acceleration (absolute) "u" and the frequency response of displacement (relative) "μ". **Figure 7a** exhibits that the m_s for points 1 and 2 are relatively similar at the lower frequency ratio (r), while the m_s for point 3 represents a better plot. **Figure 7b** shows the relative displacement of transmissibility's amplitude (η) for point 1 in frequency ratio (r). But, it was bad at the first resonant frequency ratio. The system behavior of comprehensive dynamic parameters at these three points can be seen in **Table 3**.

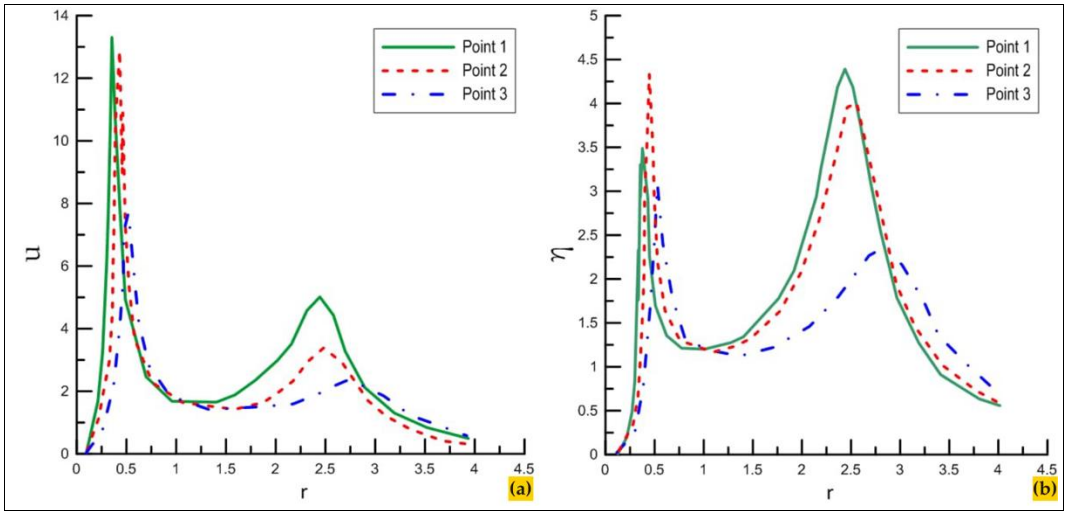

Figure 7. (a) SM absolute acceleration frequency response $\mu(r)$; (b) SM relative displacement transmissibility's amplitude $\eta(r)$

Table 3. Numerical dynamic parameters of three different suspensions based on different points

	U	Φ	ε_1	ε_2	ε_3	ε_4
Point 1	6.116	15.54	0.15	5.18	0.2	1.8
Point 2	6.116	11.97	0.15	7	0.2	1.8
Point 3	1.463	15.54	0.15	3	0.2	0.75

Figure 8a shows that the SM displacement transmissibility's amplitude μ for point 3 is much better than others. To compare the optimal design from any domain, starting a study on the transient base excitation is reasonable. **Figure 8b** shows the quarter cars' model responses to the unit step input. The reaction for points 2 and 3 is better than that for point 1. Damping time in points 1 and 2 are almost equal because they have the same RMS of SM acceleration. Point 3 damp very fast from 1 and 2 because the RMS of SM acceleration in point 3 is lower than others.

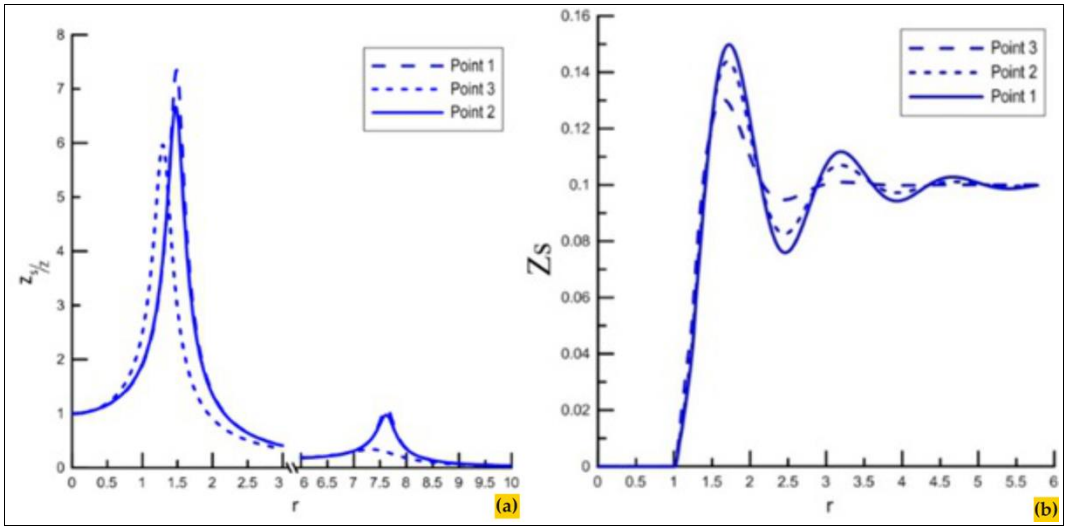

Figure 8. (a) SM displacement transmissibility's amplitude $\mu(r)$, for three different suspensions; (b) Three different suspensions step response

3.3. Handling Criteria Optimization

In the preceding section, the suspension was optimized with a focus on decreasing the SM acceleration, as opposed to wheel travel. Now, the objective is to optimize the system by enhancing the holding force, rather than wheel travel. To achieve this, ε_1 and ε_3 are initially regarded as constants, while ε_2 and ε_4 are treated as the design variables. Simultaneously, for a given mass ratio, an air spring configuration is introduced into the system, and the optimal values for reservoir tank volume and orifice resistance are derived. Subsequently, an investigation is conducted on the values of ε_1 and ε_3 through the optimization method. The RMS of the absolute holding force, denoted as γ, was computed:

$$\gamma = \sqrt{\frac{1}{\omega_2 - \omega_1}\int_{\omega_1}^{\omega_2} \tau^2 d\omega} \tag{39}$$

The plot of the SM absolute holding force (γ) for different design parameters appears in **Figure 9a**. It shows that $\gamma = \gamma(\Phi)$ with a minimum for constants ε_1 and ε_3 and variables ε_2 and ε_4. The point of minima introduces the optimum damping for the system. By the line of minima, the optimality condition is satisfied. Points alighted on the line of minima refer to a specific suspension with as low as possible accelerations for a particular value of force holding is minimum. The system's behavior analysis of three different conditions displayed in **Figure 9b** is initiated and illustrates the curve in optimum concerning γ - Φ plane, where Point 1 signifies a random point, while Points 2 and 3 represent the alternative within the minima's line. The displacement relatives among Points 1 and Point 3 are identical, while the holding force RMS for the others Points 1 and Point 2 are equivalent. In line with our optimal prediction, it is expected that the suspension's behaviour at Point 1 will be less favourable compared to Points 2 and 3. The system dynamic parameters for these points (Point 1, Point 2, and Point 3) are detailed in **Table 4**.

Table 4. Three suspensions with numerical dynamic parameters

	Φ	γ	ε_1	ε_2	ε_3	ε_4
Point 1	4.90	14.53	0.2	3	0.15	1
Point 2	8.87	17.15	0.2	2	0.15	0.72
Point 3	4.90	43.87	0.2	5	0.15	1.73

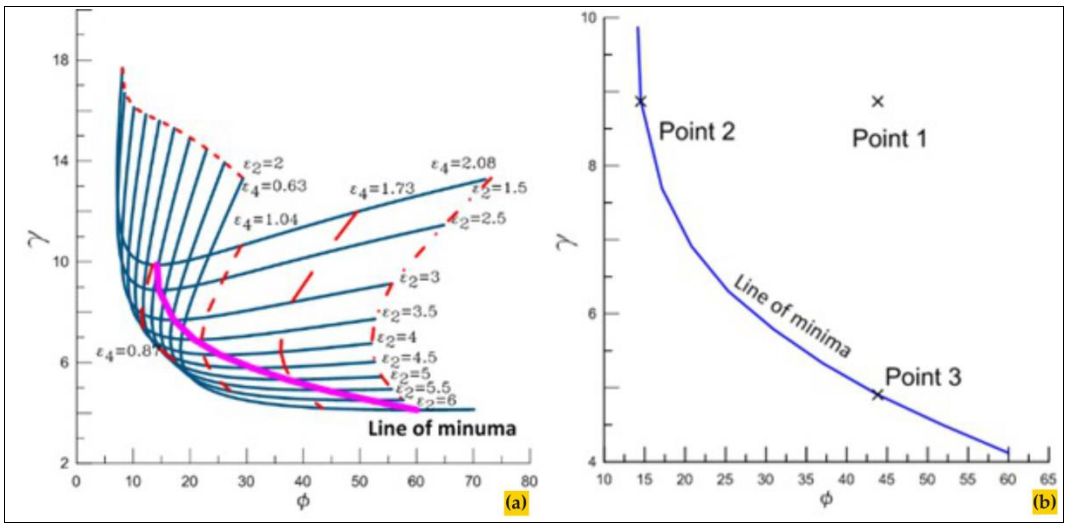

Figure 9. (a) Contour plot of $\gamma = \gamma(\Phi)$ for different values of design parameter (ε_4); (b) Two suspensions of optimal alternatives (Point 2 and Point 3), and Point 1 for a suspension under off-optimal

The effects of ε_1 and ε_3 on the model's response are shown in **Figure 10**. By increasing the value of ε_3, the RMS of absolute SM acceleration (U) and the RMS of relative displacement (Φ) decrease. The reduction in U and Φ indicates an enhancement in the vehicle's ride and HP. Additionally, an increase in ε_1 improves handling quality, while an increase in ε_3 diminishes handling quality. The results of the optimization via verification can be done numerically through simulation to examine the system behavior of the frequency response using the optimal parameters. Thus, the system is adapted to the applied base excitation harmonically and then illustrates the system frequency response.

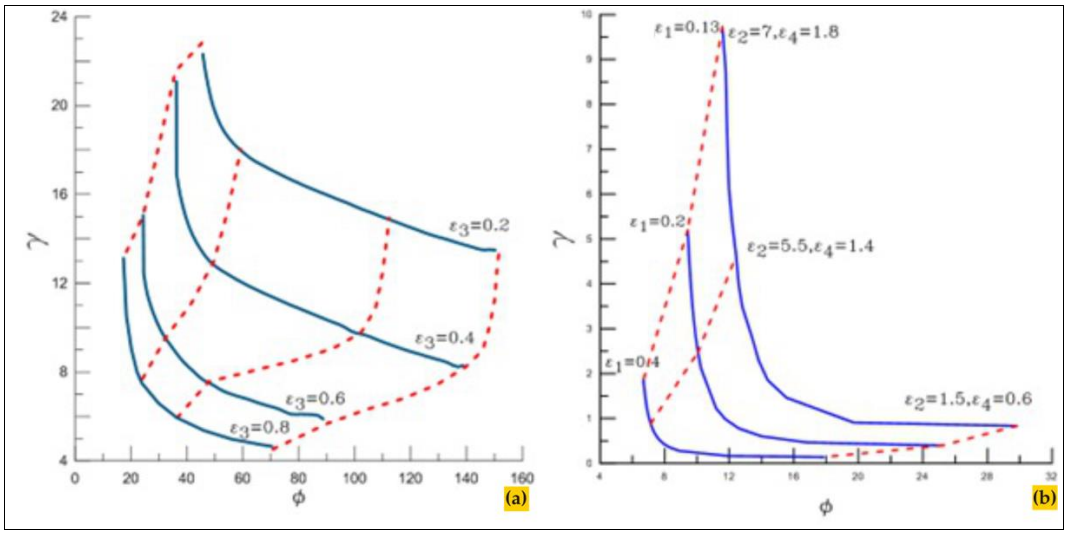

Figure 10. (a) Contour plot of $\gamma = \gamma(\Phi)$ for different values of ε_3; (b) Contour curves of the function $\gamma = \gamma(\Phi)$ for constant ε_2 and ε_4 for different values of ε_1

In **Figure 11a**, it is observed that the amplitudes of the SM relative displacement transmissibility for points 2 and 3 are equal, whereas the amplitude of the SM relative displacement transmissibility at point 1 is significantly higher than the others. As a result, the ride quality of suspension 3 surpasses the others. The figure illustrates the equality of the relative displacement transmissibility's amplitude η for points 2 and 3. Point 3 exhibits a considerably greater wheel travel displacement while the wheel travel displacement of points 1 and 2 remains identical. To enable a comparative analysis of the optimal design in another domain, investigating transient base excitation is warranted. **Figure 11b** illustrates that the holding force at points 1 and 2 is substantially higher than at point 3. Consequently, the HP of suspensions 2 and 3 outperforms the others. Points 1 and 2 exhibit nearly identical damping times due to their equal RMS of SM acceleration. In contrast, point 3 experiences significantly faster damping compared to points 1 and 2, owing to its lower RMS of SM acceleration.

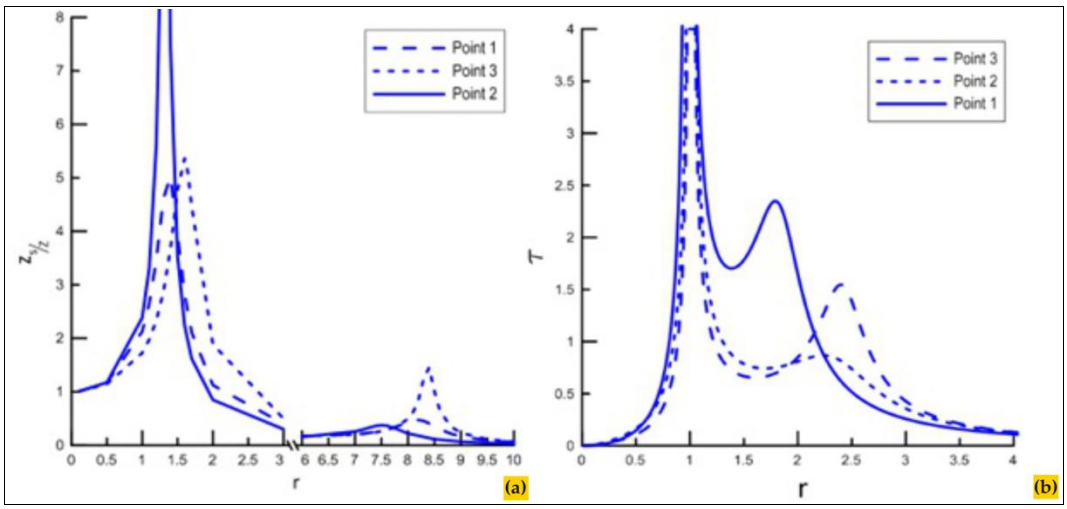

Figure 11. (a) SM relative displacement transmissibility's amplitude $\eta(r)$, for three different suspensions; (b) Holding force $\tau(r)$, for three different suspensions

3.4. Handling Criteria and Ride Optimization

In the preceding sections, the optimization process concentrated on minimizing the acceleration of the sprung mass (SM) concerning wheel travel, whereas the previous section emphasized optimizing the holding force relative to wheel travel. Augmenting wheel travel diminishes the acceleration of the SM, consequently improving the ride quality of the vehicle. However, this augmentation also leads to a reduction in holding force, which impacts the handling of the vehicle. Optimal values for ε_2 and ε_4 are determined using two optimization methods. The results demonstrate that increasing ε_2 and ε_4 enhances handling but diminishes ride quality. **Figure 12a** illustrates a specific point, designated as point 1, where both handling and ride quality are optimal. According to our optimal prediction, the behaviour of the suspension in terms of handling at point 1 is anticipated to be less favorable compared to points 2 and 3, while the behaviour of the suspension in terms of ride quality at point 1 is expected to be superior to points 2 and 3. Point 3 exhibits optimal ride quality, while point 2 demonstrates optimal handling quality. In contrast, point 1 showcases optimal qualities for both riding and handling. Consequently, by calculating AS design parameters based on ε_2 and ε_4 at point 1, an optimal combination of ride and handling can be achieved. Manipulating ε_3 in **Figure 12a** results in a shift of the optimal point, as depicted in **Figure 12b**. This curve represents the locus of optimal points based on handling and ride quality criteria.

3.5. Simulation

The performance of each optimization technique can be judged by comparing the corresponding frequency responses of the two methods which are achieved through numerical simulation. **Figure 13** and **Figure 14** respectively show the time response of SM relative displacement (Z_s/Z), time response of holding force, and time response of SM acceleration. **Figure 13a** shows that point 2 has maximum relative SM displacement and point 2 has minimum relative SM displacement. **Figure 13b** shows that point 2 has maximum holding force and point 3 has holding force therefore point 2 handling is better than point 1 and 3.

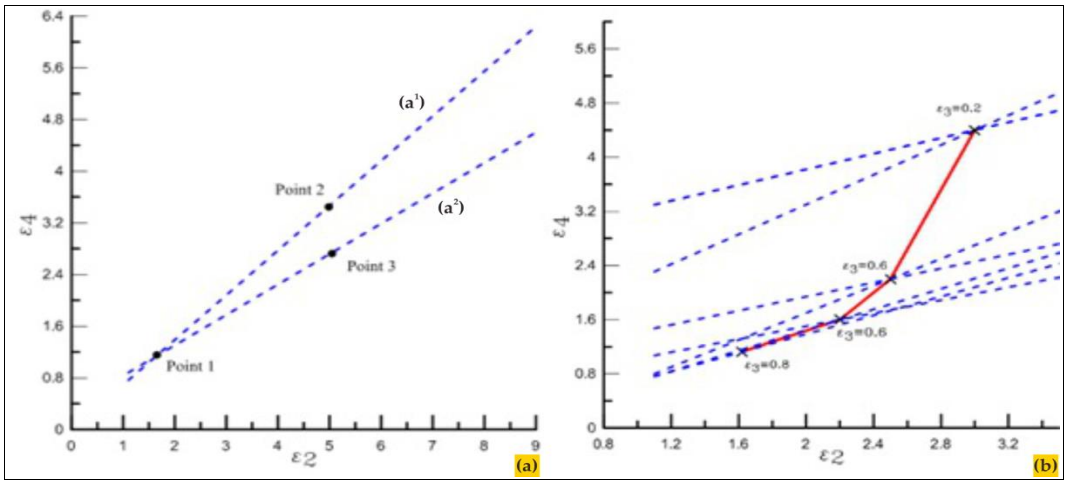

Figure 12. (a) Holding force $\tau(r)$, for three different suspensions (a^1) RMS method based on handling criteria; (a^2) RMS method based on the ride criteria; (b) Contour curves of optimal point based on the ride and handling for different values of ε_3

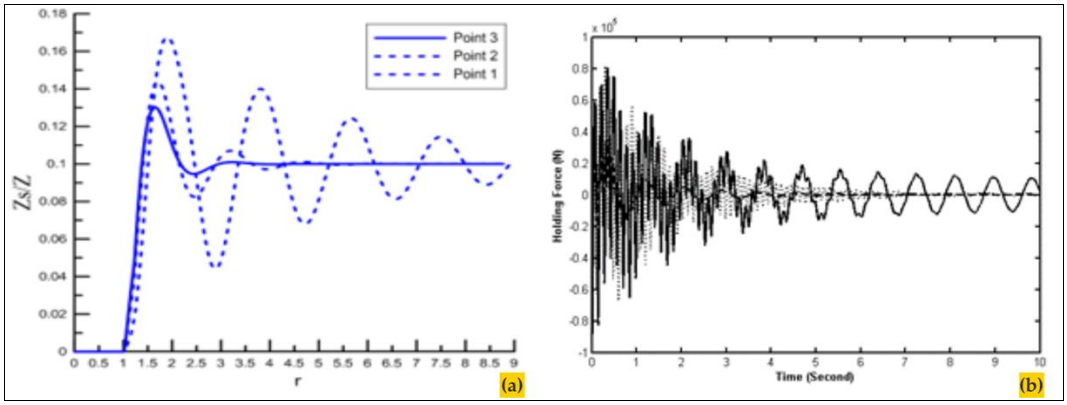

Figure 13. (a) Time response against a unit step for three different Points of suspension in SM displacement; (b) Time response to a unit step for three different Points of suspension in holding force

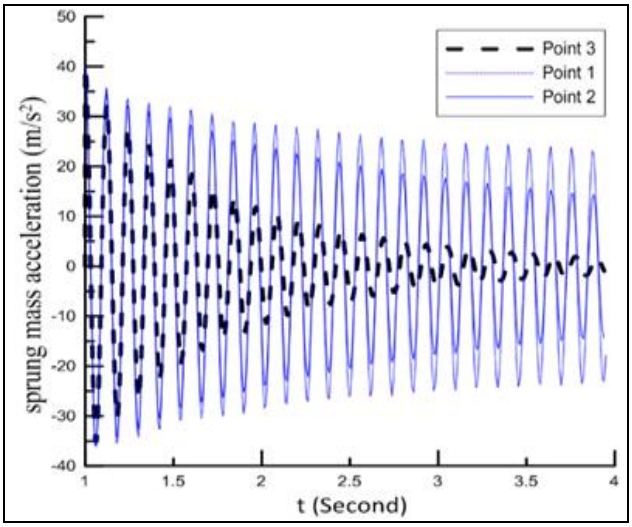

Figure 14. Time response to a unit step for three different Points of suspension in SM acceleration

Figure 14 shows that point 3 has a minimum SM acceleration than points 1 and 2 therefore point 1 ride quality is better than points 1 and 2, also point 2 ride quality is worse than point 1. According to **Figure 13b**, the handling of point 1 is mediocre for points 1 and 2. Also, according to **Figure 14**, the ride quality of point 1 is mediocre for points 1 and 2 therefore handling and ride quality of point 1 is mediocre of other point.

Very likely, a novelty from a study is in the method section, even though the topic is the same as previous studies. New methods that are simpler but have the same ability to answer research questions are superior so that they can be replicated or applied by subsequent researchers. In addition, if the equipment has accuracy tolerance in reading data such as a thermocouple, transducer, airflow meter, etc., it must also be stated clearly and honestly in the method section.

The accuracy and reliability of the results were verified through a multi-step validation process. First, the simulation outputs for ride comfort and handling performance metrics were cross-referenced with known performance benchmarks for air suspension systems. Furthermore, multiple simulation runs were conducted under varied initial conditions to confirm consistency in results, thereby enhancing reliability. Comparison with the baseline data of conventional suspension systems further validated that the proposed RMS-optimized air suspension significantly improves ride comfort (with a 45% reduction in vibration transmission) and handling stability (with an 18% increase). This rigorous validation confirms the robustness of the proposed method across different driving scenarios."

4. Conclusion

In this study, a nonlinear two DOF air suspended quarter car system and its linearized form were presented. After that, the analytical approach was utilized to predict the natural frequencies and transmissibility functions of the presented linear model. Also, the dimensionless form of the linearized model was provided. This form is suitable for the optimization process. The two-root mean square (RMS) methods of absolute sprung-mass (SM) acceleration (U) and relative displacement (Φ) were applied in the optimization procedure on the ride and the handling system in the two DOF models. Then combining the two methods we obtain a point for a specific vehicle and a curve for the unspecified vehicle that handling and ride are optimum.

In order to verify our optimization method on handling and riding, we compared the consequent vibrational behaviours of the system at the optimum points based on the ride and handling with other optimal points based on handling and ride separately. Results show that using the RMS method based on the handling and ride for this suspension has advantages in terms of reduced SM acceleration and increased handling together. The comparison demonstrates

significantly improved performance of the RMS optimized system. This allows experts to explore a wide range of design parameters efficiently.

The findings indicate that the value of the "U" parameter, representing ride quality, decreased by 76% from the first to the third point. Conversely, the "Φ" parameter, indicating stability, decreased by 22.98% from the first to the second point. This suggests that the third point offers the highest level of ride comfort, while the second point exhibits the greatest stability. The stability level at the first point equals that of the third point, but it experiences a 76% decrease in ride comfort compared to the third point. Similarly, in terms of ride comfort, the first point is on par with the second point, but it encounters a 23% decrease in stability compared to the second point.

Future research should further explore the adaptability of the RMS optimization method under varied road conditions and diverse vehicle configurations. In particular, extending the current model to include adaptive neural control systems could allow for real-time adjustments based on dynamic input from sensors, enhancing both ride comfort and handling performance. Additionally, investigating multi-objective optimizations that consider energy efficiency alongside ride and handling would offer valuable insights, particularly for electric and hybrid vehicles. These directions hold promise for advancing air suspension technology in response to the evolving demands of the automotive industry.

Acknowledgments

The authors especially would like to thank the Engineering Faculty and LPPM of the Universitas Pembangunan Nasional “Veteran”, Jakarta, Indonesia, for the internal research grant scheme of RIKIN 2024 awarded, Department of Mechanical Engineering, Islamic Azad University, Khomeinishahr, Iran, Faculty of Technology, De Montfort University, Leicester, United Kingdom, and College of Engineering, for the support given in the collaboration.

Authors’ Declaration

Authors’ contributions and responsibilities - The authors made substantial contributions to the conception and design of the study. The authors took responsibility for data analysis, interpretation, and discussion of results. The authors read and approved the final manuscript.

Funding – This work was supported by the Hibah Penelitian Internal (RIKIN 2024) Universitas Pembangunan Nasional Veteran Jakarta [977/UN61.0/HK.03.01/2024].

Availability of data and materials - All data is available from the authors.

Competing interests - The authors declare no competing interest.

Additional information – No additional information from the authors.

References

[1] P. Karimi Eskandary, A. Khajepour, A. Wong, and M. Ansari, “Analysis and optimization of air suspension system with independent height and stiffness tuning,” *International Journal of Automotive Technology*, vol. 17, no. 5, pp. 807–816, Oct. 2016, doi: 10.1007/s12239-016-0079-9.

[2] A. Alonso, J. G. Giménez, J. Nieto, and J. Vinolas, “Air suspension characterisation and effectiveness of a variable area orifice,” *Vehicle System Dynamics*, vol. 48, no. sup1, pp. 271–286, Dec. 2010, doi: 10.1080/00423111003731258.

[3] P. Servadio and N. P. Belfiore, “Influence of tyres characteristics and travelling speed on ride vibrations of a modern medium powered tractor Part II, Evaluation of the Health Risk,” *Agricultural Engineering International: CIGR Journal*, vol. 15, no. 4, pp. 132–138, 2013.

[4] I. Hostens and H. Ramon, “Descriptive analysis of combine cabin vibrations and their effect on the human body,” *Journal of Sound and Vibration*, vol. 266, no. 3, pp. 453–464, Sep. 2003, doi: 10.1016/S0022-460X(03)00578-9.

[5] K. Toyofuku, “Study on dynamic characteristic analysis of air spring with auxiliary chamber,” *JSAE Review*, vol. 20, no. 3, pp. 349–355, Jul. 1999, doi: 10.1016/S0389-4304(99)00032-6.

[6] G. Quaglia and M. Sorli, “Air Suspension Dimensionless Analysis and Design Procedure,”

Vehicle System Dynamics, vol. 35, no. 6, pp. 443–475, Jun. 2001, doi: 10.1076/vesd.35.6.443.2040.

[7] A. J. Nieto, A. L. Morales, A. González, J. M. Chicharro, and P. Pintado, "An analytical model of pneumatic suspensions based on an experimental characterization," *Journal of Sound and Vibration*, vol. 313, no. 1–2, pp. 290–307, Jun. 2008, doi: 10.1016/j.jsv.2007.11.027.

[8] Armansyah, J. Saedon, L. Zulaihah, A. Sudianto, S. R. Nasution, and G. G. Sinaga, "Design Parameters Optimization in CNC Machining Based on Taguchi, ANOVA, and Screening Method," *Journal of Mechanical Engineering*, vol. 12, pp. 209–224, 2023.

[9] M. Ghorbany, S. Ebrahimi-Nejad, and M. Mollajafari, "Global-guidance chaotic multi-objective particle swarm optimization method for pneumatic suspension handling and ride quality enhancement on the basis of a thermodynamic model of a full vehicle," *Proceedings of the Institution of Mechanical Engineers, Part D: Journal of Automobile Engineering*, vol. 237, no. 14, pp. 3334–3352, Dec. 2023, doi: 10.1177/09544070221148287.

[10] S. Nazemi, M. M. Tehrani, and M. Mollajafari, "GA tuned H<SUB align="right">∞ roll acceleration controller based on series active variable geometry suspension on rough roads," *International Journal of Vehicle Performance*, vol. 8, no. 2/3, p. 166, 2022, doi: 10.1504/IJVP.2022.122047.

[11] M. Y. Wu, H. Yin, X. B. Li, J. C. Lv, G. Q. Liang, and Y. T. Wei, "A new dynamic stiffness model with hysteresis of air springs based on thermodynamics," *Journal of Sound and Vibration*, vol. 521, p. 116693, Mar. 2022, doi: 10.1016/j.jsv.2021.116693.

[12] Y. Zheng, W.-B. Shangguan, and S. Rakheja, "Modeling and analysis of time-domain nonlinear characteristics of air spring with an auxiliary chamber," *Mechanical Systems and Signal Processing*, vol. 176, p. 109161, Aug. 2022, doi: 10.1016/j.ymssp.2022.109161.

[13] G. Nakhaie Jazar, R. Alkhatib, and M. F. Golnaraghi, "Root mean square optimization criterion for vibration behaviour of linear quarter car using analytical methods," *Vehicle System Dynamics*, vol. 44, no. 6, pp. 477–512, Jun. 2006, doi: 10.1080/00423110600621714.

[14] L. Gui, W. Shi, and W. Liu, "A semi-active suspension design for off-road vehicle base on Magneto-rheological technology," in *2012 9th International Conference on Fuzzy Systems and Knowledge Discovery*, 2012, pp. 2565–2568, doi: 10.1109/FSKD.2012.6234078.

[15] M. Özarslan Yatak, Ç. Hisar, and F. Şahin, "Fuzzy Logic Controller for Half Vehicle Active Suspension System: An Assessment on Ride Comfort and Road Holding," *International Journal of Automotive Science And Technology*, vol. 8, no. 2, pp. 179–187, 2024, doi: 10.30939/ijastech..1372001.

[16] S. Nazemi, M. Masih-Tehrani, and M. Mollajafari, "GT Car's CG height control on a rough road by using series active variable geometry suspension," *Journal of Theoritical and Applied Vibration and Acoustics*, vol. 6, no. 2, pp. 348–363, 2020, doi: 10.22064/tava.2021.125421.1164.

[17] A. Mesdaghi and M. Mollajafari, "Improve performance and energy efficiency of plug-in fuel cell vehicles using connected cars with V2V communication," *Energy Conversion and Management*, vol. 306, p. 118296, Apr. 2024, doi: 10.1016/j.enconman.2024.118296.

[18] M. A. Akbar, W.-O. Wong, and E. Rustighi, "A Hybrid Damper with Tunable Particle Impact Damping and Coulomb Friction," *Machines*, vol. 11, no. 5, p. 545, May 2023, doi: 10.3390/machines11050545.

[19] R. Rizal, A. Keshavarzi, Armansyah, D. Harmanto, and A. Kolahdooz, "Optimization and comparative analysis of an AISD suspension system with inerter element for enhanced ride and handling," *Proceedings of the Institution of Mechanical Engineers, Part D: Journal of Automobile Engineering*, 2024, doi: 10.1177/09544070241249517.

[20] M. Sorli, W. Franco, and S. Mauro, "Features of a lateral active pneumatic suspension in the high-speed train ETR470," in *Proceedings of the 6th UK Mechatronics Forum International Conference*, 1998, pp. 621–626.

[21] C. Ferraresi, G. Quaglia, and M. Sorli, "Force control laws for semi-active vehicular suspensions," *European Journal of Mechanical and Environmental Engineering*, vol. 42, no. 3, pp. 145–151, 1997.

[22] X. Jin, M. Z. Q. Chen, and Z. Huang, "Minimization of the beam response using inerter-based passive vibration control configurations," *International Journal of Mechanical Sciences*, vol.

119, pp. 80–87, Dec. 2016, doi: 10.1016/j.ijmecsci.2016.10.007.

[23] Y. Hu and M. Z. Q. Chen, "Performance evaluation for inerter-based dynamic vibration absorbers," *International Journal of Mechanical Sciences*, vol. 99, pp. 297–307, Aug. 2015, doi: 10.1016/j.ijmecsci.2015.06.003.

[24] E. Barredo *et al.*, "Closed-form solutions for the optimal design of inerter-based dynamic vibration absorbers," *International Journal of Mechanical Sciences*, vol. 144, pp. 41–53, Aug. 2018, doi: 10.1016/j.ijmecsci.2018.05.025.

[25] A. Kuznetsov, M. Mammadov, I. Sultan, and E. Hajilarov, "Optimization of improved suspension system with inerter device of the quarter-car model in vibration analysis," *Archive of Applied Mechanics*, vol. 81, no. 10, pp. 1427–1437, Oct. 2011, doi: 10.1007/s00419-010-0492-x.

[26] H. Zuo, K. Bi, H. Hao, and R. Ma, "Influences of ground motion parameters and structural damping on the optimum design of inerter-based tuned mass dampers," *Engineering Structures*, vol. 227, p. 111422, Jan. 2021, doi: 10.1016/j.engstruct.2020.111422.

[27] D. Williams and G. Montenegro, *Generalized Vehicle Dynamics*. SAE International, 2022.

[28] D. Pawar, "Numerical Prediction of In-Plane Vertical Dynamics (IPVD) Performance on a Quarter Car at the Pre-CAD Preliminary Stages of Product Development," *SAE International Journal of Advances and Current Practices in Mobility*, vol. 5, no. 2022-28–0396, pp. 1529–1536, 2022.

[29] L. Wu and L. Zuo, "A Novel Performance Analysis Method for a Full Vehicle Suspension Based on Quarter Car Model," in *International Design Engineering Technical Conferences and Computers and Information in Engineering Conference*, 2017, vol. 58158, p. V003T01A014.

[30] E. Fermi, *Thermodynamics*. New York: Dover Publications, 1996.

[31] B. Wang, B. Su, W. Zheng, Z. Ke, M. Lin, and Q. Wang, "Experimental study on flow rate and pressure drop characteristics in T-junction pipes under rolling conditions," *Physics of Fluids*, vol. 36, no. 4, Apr. 2024, doi: 10.1063/5.0199933.

[32] M. Avesh and R. Srivastava, "Modeling simulation and control of active suspension system in Matlab Simulink environment," in *2012 Students Conference on Engineering and Systems*, Mar. 2012, pp. 1–6, doi: 10.1109/SCES.2012.6199124.

[33] S. Palli, A. Duppala, R. C. Sharma, and L. V. V. Gopala Rao, "Dynamic Simulation of Automotive Vehicle Suspension Using MATLAB Simulink," *International Journal of Vehicle Structures and Systems*, vol. 14, no. 3, Jun. 2022, doi: 10.4273/ijvss.14.3.04.

[34] J. P. Den Hartog, *Mechanical Vibration, 3rd ed.* New York and London: McGraw-Hill Company Inc., 1947.

[35] A. C. Mitra, T. Soni, and G. R. Kiranchand, "Optimization of Automotive Suspension System by Design of Experiments: A Nonderivative Method," *Advances in Acoustics and Vibration*, vol. 2016, pp. 1–10, Jul. 2016, doi: 10.1155/2016/3259026.

[36] J. P. C. Gonçalves and J. A. C. Ambrósio, "Optimization of Vehicle Suspension Systems for Improved Comfort of Road Vehicles Using Flexible Multibody Dynamics," *Nonlinear Dynamics*, vol. 34, no. 1/2, pp. 113–131, Oct. 2003, doi: 10.1023/B:NODY.0000014555.46533.82.